Closed-form Maker fringe formulas for poled polymer thin films in multilayer structures

Dong Hun Park[*] and Warren N. Herman

Laboratory for Physical Sciences, University of Maryland, College Park, 20740, USA
[*]leomac@lps.umd.edu

Abstract: We report new closed-form expressions for Maker fringes of anisotropic and absorbing poled polymer thin films in multilayer structures that include back reflections of both fundamental and second-harmonic waves. The expressions, based on boundary conditions at each interface, can be applied to multilayer structures containing a buffer and a transparent conducting oxide layer, which might enhance multiple reflections of fundamental and second-harmonic waves inside a nonlinear thin film layer. This formulation facilitates Maker fringe analysis for a sample containing additional multilayer structures on either side of a poled polymer thin film. Experimental data and numerical simulations are given to indicate the importance of inclusion of such a reflective layer in analyses for reliable characterization of second-harmonic tensor elements.

OCIS codes: (190.4710) Optical nonlinearities in organic materials; (160.5470) Polymers; (310.6860) Thin films, optical properties.

References and links

1. G. A. Lindsay and K. D. Singer, eds., *Polymers for Second-Order Nonlinear Optics*, Vol 601 of ACS Symposium Series (ACS, 1995).
2. W. N. Herman, S. R. Flom, and S. H. Foulger, eds., *Organic Thin Films for Photonic Applications*, Vol. 1039 of ACS Symposium Series (ACS, 2010).
3. D. M. Burland, R. D. Miller, and C. A. Walsh, "Second-order nonlinearity in poled-polymer systems," Chem. Rev. **94**(1), 31–75 (1994).
4. C. C. Teng and H. T. Man, "Simple reflection technique for measuring the electro-optic coefficient of poled polymers," Appl. Phys. Lett. **56**(18), 1734–1736 (1990).
5. J. S. Schildkraut, "Determination of the electro optic coefficient of a poled polymer film," Appl. Opt. **29**(19), 2839–2841 (1990).
6. D. H. Park, C. H. Lee, and W. N. Herman, "Analysis of multiple reflection effects in reflective measurements of electro-optic coefficients of poled polymers in multilayer structures," Opt. Express **14**(19), 8866–8884 (2006).
7. P. D. Maker, R. W. Terhune, M. Nisenhoff, and C. M. Savage, "Effects of Dispersion and focusing on the production of optical harmonics," Phys. Rev. Lett. **8**(1), 21–22 (1962).
8. J. Jerphagnon and S. K. Kurtz, "Maker fringes: a detailed comparison of theory and experiment for isotropic and uniaxial crystals," J. Appl. Phys. **41**(4), 1667–1681 (1970).
9. N. Okamoto, Y. Hirano, and O. Sugihara, "Precise estimation of nonlinear-optical coefficients for anisotropic nonlinear films with $C_{\infty v}$ symmetry," J. Opt. Soc. Am. B **9**(11), 2083–2087 (1970).
10. W. N. Herman and L. M. Hayden, "Maker fringes revisited: second-harmonic generation from birefringent or absorbing materials," J. Opt. Soc. Am. B **12**(3), 416–427 (1995).
11. T. K. Lim, M.-Y. Jeong, C. Song, and D. C. Kim, "Absorption effect in the calculation of a second-order nonlinear coefficient from the data of a maker fringe experiment," Appl. Opt. **37**(13), 2723–2728 (1998).
12. H. Hellwig and L. Bohaty, "Multiple reflections and Fabry-Perot interference corrections in Maker fringe experiments," Opt. Commun. **161**(1-3), 51–56 (1999).
13. N. A. Sanford and J. A. Aust, "Nonlinear optical characterization of $LiNbO_3$. I. Theoretical analysis of Maker fringe patterns for x-cut wafers," J. Opt. Soc. Am. B **15**(12), 2885–2908 (1998).
14. M. Abe, I. Shoji, J. Suda, and T. Kondo, "Comprehensive analysis of multiple-reflection effects on rotational Maker-fringe experiments," J. Opt. Soc. Am. B **25**(10), 1616–1624 (2008).
15. M. Braun, F. Bauer, Th. Vogtmann, and M. Schwoerer, "Precise second-harmonic generation Maker fringe measurements in single crystals of the diacetylene NP/4-MPU and evaluation by a second-harmonic generation theory in 4×4 matrix formulation and ray tracing," J. Opt. Soc. Am. B **14**(7), 1699–1706 (1997).
16. M. Braun, F. Bauer, Th. Vogtmann, and M. Schwoerer, "Detailed analysis of second-harmonic-generation Maker fringes in biaxially birefringent materials by a 4×4 matrix formulation," J. Opt. Soc. Am. B **15**(12), 2877–2884 (1998).

#157751 - $15.00 USD Received 7 Nov 2011; revised 9 Dec 2011; accepted 12 Dec 2011; published 19 Dec 2011

17. V. Rodriguez and C. Sourisseau, "General Maker-fringe ellipsometric analyses in multilayer nonlinear and linear anisotropic optical media," J. Opt. Soc. Am. B **19**(11), 2650–2664 (2002).
18. S. Lee, B. Park, S.-D. Lee, G. Park, and Y. D. Kim, "Second-harmonic generation in poled films of nonlinear optical polymer composites," Opt. Quantum Electron. **27**(5), 411–420 (1995).
19. I. P. Kaminow, *An Introduction to Electrooptic Devices* (Academic, 1974).
20. J. P. Drummond, S. J. Clarson, J. S. Zetts, F. K. Hopkins, and S. J. Caracci, "Enhanced electro-optic poling in guest–host systems using conductive polymer-based cladding layers," Appl. Phys. Lett. **74**(3), 368–370 (1999).
21. M. Born and E. Wolf, *Principles of Optics,* 7th ed. (Cambridge University Press, 1999).
22. P. Yeh, *Optical Waves in Layered Media* (Wiley, 1988)
23. D. Guo, R. Lin, and W. Wang, "Gaussian-optics-based optical modeling and characterization of a Fabry-Perot microcavity for sensing applications," J. Opt. Soc. Am. A **22**(8), 1577–1588 (2005).
24. K. D. Singer, M. D. Kuzyk, and J. E. Sohn, "Second-order nonlinear-optical processes in orientationally ordered materials: relationship between molecular and macroscopic properties," J. Opt. Soc. Am. B **17**, 566–571 (2000).
25. R. C. Hoffman, A. G. Mott, M. J. Ferry, T. M. Pritchett, W. Shensky, J. A. Orlicki, G. R. Martin, J. Dougherty, J. L. Leadore, A. M. Rawlett, and D. H. Park, "Poling of visible chromophores in millimeter-thick PMMA host," Opt. Mater. Express **1**(1), 67–77 (2011).
26. J. Zhang, G. Wang, Z. Liu, L. Wang, G. Zhang, X. Zhang, Y. Wu, P. Fu, and Y. Wu, "Growth and optical properties of a new nonlinear $Na_3La_9O_3(BO_3)_8$ crystal," Opt. Express **18**(1), 237–243 (2010).
27. C. Chen, Z. Shao, J. Jiang, J. Wei, J. Lin, J. Wang, N. Ye, J. Lv, B. Wu, M. Jiang, M. Yoshimura, Y. Mori, and T. Sasaki, "Determination of the nonlinear optical coefficients of $YCa_4O(BO_3)_3$ crystal," J. Opt. Soc. Am. B **17**(4), 566–571 (2000).
28. S. Ramo, J. R. Whinnery, and T. V. Duzer, *Fields and Waves in Communication Electronics* (Wiley, New York, 1965), Chap. 6.

1. Introduction

Nonlinear optical polymers (NLOP) based on second-order nonlinearity have been widely studied because they are a class of photonic material that could substitute for inorganic nonlinear crystals in high speed optical communication and signal processing [1,2]. Techniques commonly used to obtain a macroscopic second-order nonlinear optical (NLO) response include corona and electrode contact poling methods [1–3]. The setup for electrode contact poling is somewhat simpler than for corona poling, but requires two electrodes on both sides of the NLOP to apply voltage. Various methods for characterization of second-order electro-optic (EO) effects [4–6] and second-harmonic generation (SHG) [7–17] have been investigated. The Maker fringe technique [7] is one of the most popular techniques used in determining the tensorial second-harmonic (SH) NLO coefficients $d_{\mu j}$ (μ = 1-3, j = 1-6) associated with SHG. This technique, as further described in detail by Jerphagnon and Kurtz [8] and Okamoto *et al*. [9], has been applied to inorganic and organic crystals as well as organic polymers for many years. However, these early formulations neglected the anisotropy or absorption of the NLO material, resulting in possible errors in the estimation of $d_{\mu j}$ for birefringent and absorbing materials. Of those that account for material anisotropy and/or absorption, most methods make an assumption of no back reflections. In 1995, Herman and Hayden (HH) [10] presented a Maker fringe formulation that takes into account either the anisotropy or the absorption of the constituent NLO materials as well as back reflection of SH waves causing multiple reflections, which correctly predicted experimental results [11]. Other formulations that account for back reflections of both fundamental and SH assume the slowly-varying amplitude approximation or partially overlapping beams by using coupled wave equations or Green's function analysis [12–14]. Matrix techniques were used to numerically solve the SH signals from an arbitrarily oriented biaxial medium [15,16] or a multilayered structure with multiple nonlinear layers [17]. Most analyses thus far have considered only a three layer structure such as air/nonlinear material/substrate or generated somewhat complicated numerical results for multilayer structures without closed-form analytical expressions. The three layer model is suitable for second-order nonlinear materials such as thick $LiNbO_3$ or a thin NLOP film on a thick substrate prepared by corona poling or other poling methods where electrodes are not necessary. However, NLOP films prepared by electrode contact poling require two additional electrode layers for application of voltage, and the transparent conducting oxide (TCO) electrode between the NLO film layer and a substrate were neglected in previous analyses [18] of such structures.

#157751 - $15.00 USD Received 7 Nov 2011; revised 9 Dec 2011; accepted 12 Dec 2011; published 19 Dec 2011

In this paper, we extend the transmission HH Maker fringe formulation 1) to account for simultaneous anisotropy and absorption of the NLO polymer, 2) a multilayer structure that includes dielectric or non-dielectric materials, and 3) back reflections of both SH and fundamental waves. Back reflections are considered because some absorbing layers, such as a TCO layer, may appreciably enhance multiple reflections. These closed-form mathematical expressions based on boundary conditions are intuitively applicable to a multilayer structure containing a single nonlinear layer with additional absorbing and/or anisotropic linear media.

We also provide a Maker fringe formulation for reflection. This is useful when a highly reflecting NLO sample is used or when a metal layer used as a poling electrode is not removed after poling. Such a formulation is expected to be useful for comparing SHG and EO measurements on the same film. We present experimental results and simulations in order to validate the proposed formulation and indicate the importance of inclusion of full layer structures with multiple reflections for reliable estimation of $d_{\mu j}$ coefficients.

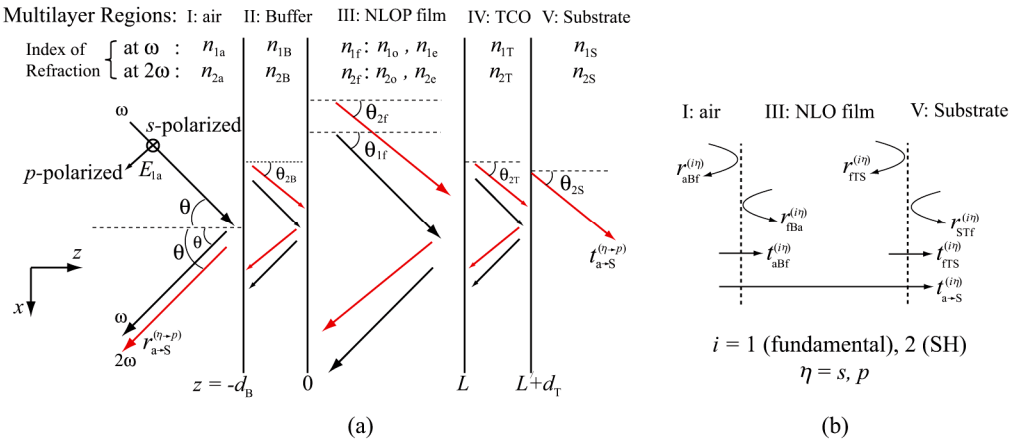

Fig. 1. (a) Multilayer structure geometry containing buffer and TCO layers. Black solid arrows represent fundamental waves and red arrows SH waves. First and second subscripts on n and θ are used to represent dependence of wavelength and layer symbols, respectively. For NLO film, o and e represent ordinary and extraordinary refractive indices, respectively. (b) Equivalent three layer structure using virtual layers (dashed lines). The numeral subscript/superscript i represents a wavelength (i = 1: fundamental and i = 2: second-harmonic). For example, $t_{a\to S}^{(1p)}$ means a p-polarization transmission coefficient from air to substrate at the fundamental (i = 1) wavelength.

2. Theory

As much as possible, we have attempted to follow the notation used in Ref. [10]. A poled organic thin film prepared by spin coating belongs to the ∞mm point-group symmetry (space group $C_{\infty v}$) and has complex ordinary and extraordinary indices of refraction, n_o and n_e, respectively [19]. The SH d-coefficient tensor contains three independent complex elements and is given by [10]

$$\vec{\mathbf{d}} = \begin{pmatrix} 0 & 0 & 0 & 0 & d_{15} & 0 \\ 0 & 0 & 0 & d_{15} & 0 & 0 \\ d_{31} & d_{31} & d_{33} & 0 & 0 & 0 \end{pmatrix}. \qquad (1)$$

Because a contact-poled thin film usually requires a substrate for support and two electrodes such as gold and TCO for both contact poling and subsequent reflective EO measurement [4–6], we consider a five-layer structure (air/buffer/NLO film/TCO/substrate) as shown in Fig. 1(a). Later we discuss generalization to more than five layers. For transmission type Maker fringe experiments, the top electrode layer on a NLO film, typically gold for

#157751 - $15.00 USD Received 7 Nov 2011; revised 9 Dec 2011; accepted 12 Dec 2011; published 19 Dec 2011

contact poling and reflective EO measurement, should be removed after the poling process using an appropriate etchant. The buffer layer might be a protection layer for efficient poling [20] or residual metal owing to imperfect etching. In the following analysis, SHG from interfaces or metal is assumed to be negligible compared with that from the poled polymer thin film. We assume that a *p*-polarized plane wave of angular frequency ω (fundamental wave) is incident from the left at an angle of incidence θ. Derivation of the incident *s*-polarized case is similar and straightforward. The SH electric (**E**) and magnetic (**H**) fields in each region are given as

$$
\begin{aligned}
&\text{Region I:} && \begin{cases} \mathbf{E}_{2a} = \hat{\mathbf{e}}_{2a}^{r} r_{a\to S}^{(p\to p)} e^{i\mathbf{k}_{2a}^{r}\cdot\mathbf{r}} \\ \mathbf{H}_{2a} = \hat{\mathbf{y}} n_{2a} r_{a\to S}^{(p\to p)} e^{i\mathbf{k}_{2a}^{r}\cdot\mathbf{r}} \end{cases} \\
&\text{Region II:} && \begin{cases} \mathbf{E}_{2B} = \hat{\mathbf{e}}_{2B} A e^{i\mathbf{k}_{2B}\cdot\mathbf{r}} + \hat{\mathbf{e}}_{2B}^{r} B e^{i\mathbf{k}_{2B}^{r}\cdot\mathbf{r}} \\ \mathbf{H}_{2B} = \hat{\mathbf{y}} n_{2B} A e^{i\mathbf{k}_{2B}\cdot\mathbf{r}} + \hat{\mathbf{y}} n_{2B} B e^{i\mathbf{k}_{2B}^{r}\cdot\mathbf{r}} \end{cases} \\
&\text{Region III:} && \begin{cases} \mathbf{E}_{2f} = \hat{\mathbf{e}}_{2f} C e^{i\mathbf{k}_{2f}\cdot\mathbf{r}} + \hat{\mathbf{e}}_{2f}^{r} D e^{i\mathbf{k}_{2f}^{r}\cdot\mathbf{r}} + \mathbf{e}_{b} e^{2i\mathbf{k}_{1f}\cdot\mathbf{r}} + \mathbf{e}_{b}^{r} e^{2i\mathbf{k}_{1f}^{r}\cdot\mathbf{r}} \\ \mathbf{H}_{2f} = \hat{\mathbf{y}} n_{2f}(\theta_{2f}) C e^{i\mathbf{k}_{2f}\cdot\mathbf{r}} + \hat{\mathbf{y}} n_{2f}(\theta_{2f}) D e^{i\mathbf{k}_{2f}^{r}\cdot\mathbf{r}} + \mathbf{h}_{b} e^{2i\mathbf{k}_{1f}\cdot\mathbf{r}} + \mathbf{h}_{b}^{r} e^{2i\mathbf{k}_{1f}^{r}\cdot\mathbf{r}} \end{cases} \\
&\text{Region IV:} && \begin{cases} \mathbf{E}_{2T} = \hat{\mathbf{e}}_{2T} E e^{i\mathbf{k}_{2T}\cdot\mathbf{r}} + \hat{\mathbf{e}}_{2T}^{r} F e^{i\mathbf{k}_{2T}^{r}\cdot\mathbf{r}} \\ \mathbf{H}_{2T} = \hat{\mathbf{y}} n_{2T} E e^{i\mathbf{k}_{2T}\cdot\mathbf{r}} + \hat{\mathbf{y}} n_{2T} F e^{i\mathbf{k}_{2T}^{r}\cdot\mathbf{r}} \end{cases} \\
&\text{Region V:} && \begin{cases} \mathbf{E}_{2S} = \hat{\mathbf{e}}_{2S} t_{a\to S}^{(p\to p)} e^{i\mathbf{k}_{2S}\cdot\mathbf{r}} \\ \mathbf{H}_{2S} = \hat{\mathbf{y}} n_{2S} t_{a\to S}^{(p\to p)} e^{i\mathbf{k}_{2S}\cdot\mathbf{r}}, \end{cases}
\end{aligned}
\tag{2}
$$

where $r_{a\to S}^{(p\to p)}$ and $t_{a\to S}^{(p\to p)}$ represent SH *p*-wave reflection and transmission coefficients, respectively ($p\to p$: fundamental *p*-wave input to SH *p*-wave output, $s\to p$: fundamental *s*-wave input to SH *p*-wave output) and *A*, *B*, *C*, *D*, *E*, and *F* are constants. In case of isotropic layers, $\hat{\mathbf{e}}_{2l} = (\cos\theta_{2l}, 0, -\sin\theta_{2l})$ and $\hat{\mathbf{e}}_{2l}^{r} = (-\cos\theta_{2l}, 0, -\sin\theta_{2l})$ are the polarization unit vectors for the electric fields of the transmitted and reflected SH waves, respectively, at layer $l = a, B, f, T, S$ representing air, buffer, NLO film, TCO, and substrate, respectively, and $\hat{\mathbf{y}} = (0,1,0)$ is the unit vector for the magnetic field **H**. In the anisotropic layers, the unit vectors along the SH electric field directions are $\hat{\mathbf{e}}_{2l} = \left(\cos\left(\theta_{2l} - \gamma_{2l}\right), 0, -\sin\left(\theta_{2l} - \gamma_{2l}\right)\right)$ and $\hat{\mathbf{e}}_{2l}^{r} = \left(-\cos\left(\theta_{2l} - \gamma_{2l}\right), 0, -\sin\left(\theta_{2l} - \gamma_{2l}\right)\right)$, where the walk-off angles γ_{il} at the fundamental (*i* = 1) and SH (*i* = 2) wavelengths are included because of birefringence of the anisotropic layers [10]. Similarly, $\mathbf{k}_{2l} = 2k_0 n_{2l}(\sin\theta_{2l}, 0, \cos\theta_{2l})$ and $\mathbf{k}_{2l}^{r} = 2k_0 n_{2l}(\sin\theta_{2l}, 0, -\cos\theta_{2l})$ are wave vectors for the forward and backward SH waves, respectively. Here, $k_0 = 2\pi/\lambda = \omega/c$ is the wave vector of the fundamental in free space. n_{1l} and n_{2l} are indices of refraction of the layer *l* at the fundamental and SH wavelengths, respectively. For birefringent NLO films, we have for *p*-polarization

$$
n_{if}(\theta_{if}) = \left(\frac{\cos^2\theta_{if}}{n_{io}^2} + \frac{\sin^2\theta_{if}}{n_{ie}^2} \right)^{-1/2}, \tag{3}
$$

where $i = 1, 2$ [21,22]. We have omitted the subscript for layer information in the anisotropic indices, n_{io} and n_{ie}, to prevent the notation from becoming unduly cumbersome, but Eq. (3) also can be applied to other anisotropic layers. The bound waves [8,9] $\mathbf{e}_b$, $\mathbf{e}_b^{r}$, $\mathbf{h}_b$, and $\mathbf{h}_b^{r}$ in

#157751 - $15.00 USD Received 7 Nov 2011; revised 9 Dec 2011; accepted 12 Dec 2011; published 19 Dec 2011

region III are inhomogeneous solutions that satisfy Maxwell's equation given in Eq. (A1). A detailed description for these bound waves is given in Appendix A.

Continuity of tangential **E** and **H** components at each interface gives the boundary conditions. The matrix method employing multiple interface boundary conditions [22] is used to calculate $t_{a\to S}^{(p\to p)}$ and $r_{a\to S}^{(p\to p)}$, which are the *p*-wave SH transmission and reflection coefficients, respectively for the case of a fundamental *p*-wave input. From Eq. (B3), we find that the SH transmission coefficient from the multilayer structure containing an absorptive and birefringent NLO film is given as

$$t_{a\to S}^{(\eta\to p)} = -e^{-i(\phi_{2SL}+\phi_{2ST})}\frac{4\pi i k_0 L}{n_{2f}c_{\gamma_2}c_{2-\gamma}}\left[\frac{t_{a\to S}^{(1\eta)}E_{1a}}{t_{fTS}^{(1\eta)}}\right]^2\frac{t_{a\to S}^{(2p)}}{t_{aBf}^{(2p)}} \times\left\{\begin{array}{l} d_{eff}^{(\eta\to p)}\left[e^{-i\Phi^{(\eta\to p)}}+r_{fBa}^{(2p)}\left(r_{fTS}^{(1\eta)}\right)^2 e^{i\Phi^{(\eta\to p)}}\right]\sin c(\Psi^{(\eta\to p)}) \\ +d_{eff}^{r(\eta\to p)}\left[\left(r_{fTS}^{(1\eta)}\right)^2 e^{i\Psi^{(\eta\to p)}}+r_{fBa}^{(2p)}e^{-i\Psi^{(\eta\to p)}}\right]\sin c(\Phi^{(\eta\to p)}) \end{array}\right\}, \quad (4)$$

where $c_{\gamma_2}=\cos\gamma_{2f}$, $\eta = s, p$, and E_{1a} is the electric field of the incident fundamental wave. $\Psi^{(\eta\to\mu)}$ and $\Phi^{(\eta\to\mu)}$ are defined as

$$\Psi^{(\eta\to\mu)} = \phi_1^{(\eta)} - \frac{\phi_2^{(\mu)}}{2},\ \Phi^{(\eta\to\mu)} = \phi_1^{(\eta)} + \frac{\phi_2^{(\mu)}}{2}. \quad (5)$$

where $\mu = s, p$ and the phase terms are $\phi_1^{(p)} = k_0 n_{1f}(\theta_{1f})\cos\left(\theta_{1f}\right)L$, $\phi_1^{(s)} = k_0 n_{1o}\cos\left(\theta_{1f}^{(s)}\right)L$, and $\phi_2^{(p)} = 2k_0 n_{2f}(\theta_{2f})\cos\left(\theta_{2f}\right)L$. Equation (4) can be rewritten using the identity $n_{2f}c_{\gamma_2}c_{2-\gamma}\big/\left(n_{2a}c_{2a}\right) = t_{fBa}^{(2p)}\big/t_{aBf}^{(2p)}$. Note that in comparison with the HH theory [10], Eq. (4) reduces to the HH equation when the Fresnel reflection coefficient of the fundamental wave $r_{fTS}^{(1\eta)}$ is zero and the buffer and TCO layers do not exist. The detailed derivations are given in Appendix B. Finally, the transmitted SH power is given by

$$P_{2\omega} = \frac{c}{8\pi}\left(t_{Sa}^{(2p)}\right)^2\left|t_{a\to S}^{(\eta\to p)}\right|^2 A_{cross}, \quad (6)$$

where $t_{Sa}^{(2p)}$ is the *p*-polarized transmission coefficient of the SH wave at the substrate/air interface and A_{cross} is the cross-sectional area of the fundamental wave.

We notice that the SH transmission coefficient is proportional to $t_{a\to S}^{(2p)}\big/t_{aBf}^{(2p)}$ and to $\left(t_{a\to S}^{(1\eta)}\big/t_{fTS}^{(1\eta)}\right)^2$. Thus, the SH transmission can be maximized by increasing $t_{a\to S}^{(2p)}$ and $t_{a\to S}^{(1\eta)}$ while $t_{aBf}^{(2p)}$ and $t_{fTS}^{(1\eta)}$ are decreased. As seen from Eqs. (B1)-(B4), the mathematical expression can easily be modified to apply to a multilayered structure containing additional layers on either side of the NLO film by simply substituting the appropriate transmission and reflection coefficients at virtual layers [23] and adding a phase term introduced by the additional layers. Then, we have

$$t_{a\to S}^{(\eta\to p)} = -e^{-2ik_0 n_{2S}c_{2S}(L+d_T+l_{AD})}\frac{4\pi i k_0 L}{n_{2f}c_{\gamma_2}c_{2-\gamma}}\left[\frac{t_{a\to S}^{(1\eta)}E_{1a}}{t_{f\to S}^{(1\eta)}}\right]^2\frac{t_{a\to S}^{(2p)}}{t_{a\to f}^{(2p)}} \times\left\{\begin{array}{l} d_{eff}^{(\eta\to p)}\left[e^{-i\Phi^{(\eta\to p)}}+r_{f\to a}^{(2p)}\left(r_{f\to S}^{(1\eta)}\right)^2 e^{i\Phi^{(\eta\to p)}}\right]\sin c(\Psi^{(\eta\to p)}) \\ +d_{eff}^{r(\eta\to p)}\left[\left(r_{f\to S}^{(1\eta)}\right)^2 e^{i\Psi^{(\eta\to p)}}+r_{f\to a}^{(2p)}e^{-i\Psi^{(\eta\to p)}}\right]\sin c(\Phi^{(\eta\to p)}) \end{array}\right\}, \quad (7)$$

#157751 - $15.00 USD Received 7 Nov 2011; revised 9 Dec 2011; accepted 12 Dec 2011; published 19 Dec 2011

where $r_{j\to k}^{(i\eta)}$ represents an η-polarization Fresnel reflection coefficient from j layer to k layer as described in Eqs. (B5)-(B8). l_{AD} is the thickness of an additional layer located between the NLO film and the substrate, but the phase factor resulting from the additional layer doesn't affect the magnitude of SH transmittance. Again, each side of the multilayer structure on a NLOP film can be treated as a single virtual interface as shown in Fig. 1(b). We note again that these equations do not apply to a sample containing multiple nonlinear film layers.

As briefly mentioned in Section 1, a metal electrode layer such as gold is usually removed after poling for the transmission type of Maker fringe experiment. It can however be used as a reflector without a metal removal process, which allows us to re-pole the sample or to use it for another reflection type of measurement. A formula for the SH reflection coefficient can be obtained from Eq. (B3) and is given by

$$
\begin{aligned}
r_{a\to S}^{(\eta\to p)} = & -e^{-i\phi_{2aB}}\left(\frac{t_{a\to S}^{(1\eta)}E_{1a}}{t_{fTS}^{(1\eta)}}\right)^2 \frac{4\pi i k_0 L}{n_{2f}c_{\gamma_2}c_{2-\gamma}t_{aBf}^{(2p)}} \\
& \times\left\{ r_{a\to S}^{(2p)}\begin{bmatrix} d_{eff}^{(\eta\to p)}\left(e^{-i\Phi^{(\eta\to p)}}+r_{fBa}^{(2p)}\left(r_{fTS}^{(1\eta)}\right)^2 e^{i\Phi^{(\eta\to p)}}\right)\sin c(\Psi^{(\eta\to p)}) \\ +d_{eff}^{r(\eta\to p)}\left(r_{fBa}^{(2p)}e^{-i\Psi^{(\eta\to p)}}+\left(r_{fTS}^{(1\eta)}\right)^2 e^{i\Psi^{(\eta\to p)}}\right)\sin c(\Phi^{(\eta\to p)}) \end{bmatrix}\right. \\
& \left. -\begin{bmatrix} d_{eff}^{(\eta\to p)}\left(r_{aBf}^{(2p)}e^{-i\Phi^{(\eta\to p)}}+\left(r_{aBf}^{(2p)}r_{fBa}^{(2p)}-t_{aBf}^{(2p)}t_{fBa}^{(2p)}\right)\left(r_{fTS}^{(1\eta)}\right)^2 e^{i\Phi^{(\eta\to p)}}\right)\mathrm{sinc}(\Psi^{(\eta\to p)}) \\ +d_{eff}^{r(\eta\to p)}\left(\left(r_{aBf}^{(2p)}r_{fBa}^{(2p)}-t_{aBf}^{(2p)}t_{fBa}^{(2p)}\right)e^{-i\Psi^{(\eta\to p)}}+r_{aBf}^{(2p)}\left(r_{fTS}^{(1\eta)}\right)^2 e^{i\Psi^{(\eta\to p)}}\right)\mathrm{sinc}(\Phi^{(\eta\to p)}) \end{bmatrix}\right\},
\end{aligned}
\tag{8}
$$

where $r_{aBf}^{(2p)}r_{fBa}^{(2p)}-t_{aBf}^{(2p)}t_{fBa}^{(2p)}$ becomes -1 in the case of no buffer layer, that is, a single interface.

3. Results

We have derived mathematical expressions for Maker fringe patterns in both transmission and reflection in the previous section. Closed-form expressions offer the advantage of easier physical interpretation and can be extended for samples containing an additional absorbing and/or anisotropic linear medium.

For the first experimental example, we measured a Maker fringe pattern ($p\to p$) for X-cut quartz (rotation is about z-axis), which is commonly used for reference. The focused incident laser spot size used in the experiment is a few tens of microns, which is much smaller than the thickness of the X-cut quartz (533 μm). Therefore, multiply reflected beams at the quartz/air interface are spatially localized, so they don't interfere. On the other hand, Eq. (4) is derived based on the plane wave analysis. One can simply make reflections $r_{fBa}^{(2p)}$ and $r_{fTS}^{(1\eta)}$ in Eq. (4) null in order to get a formulation that does not contain a back reflection effect. As shown in Fig. 2(a), a simulation (blue curve) using Eq. (4) shows large rapid SH intensity fluctuations as expected from multiple reflections in such a thick slab structure, but the measured SHG data (red dots) doesn't show these fluctuations and is well described by the modified Eq. (4) (cyan curve), where $r_{fBa}^{(2p)}$ and $r_{fTS}^{(1\eta)}$ are set equal to zero. In order to verify our formula for a multilayer structure (number of layers ≥ 4), ~5 nm thick gold was deposited on quartz (air/quartz/Au/air) using a sputtering system and the SH intensity was measured as a function of angle. Subsequently, another thin gold layer was deposited on the other side of quartz (air/Au/quartz/Au/air) and SH data again collected. The SH transmitted intensity decreases as a gold metal layer is added because of the transmission loss and the reflection caused by the

#157751 - $15.00 USD Received 7 Nov 2011; revised 9 Dec 2011; accepted 12 Dec 2011; published 19 Dec 2011

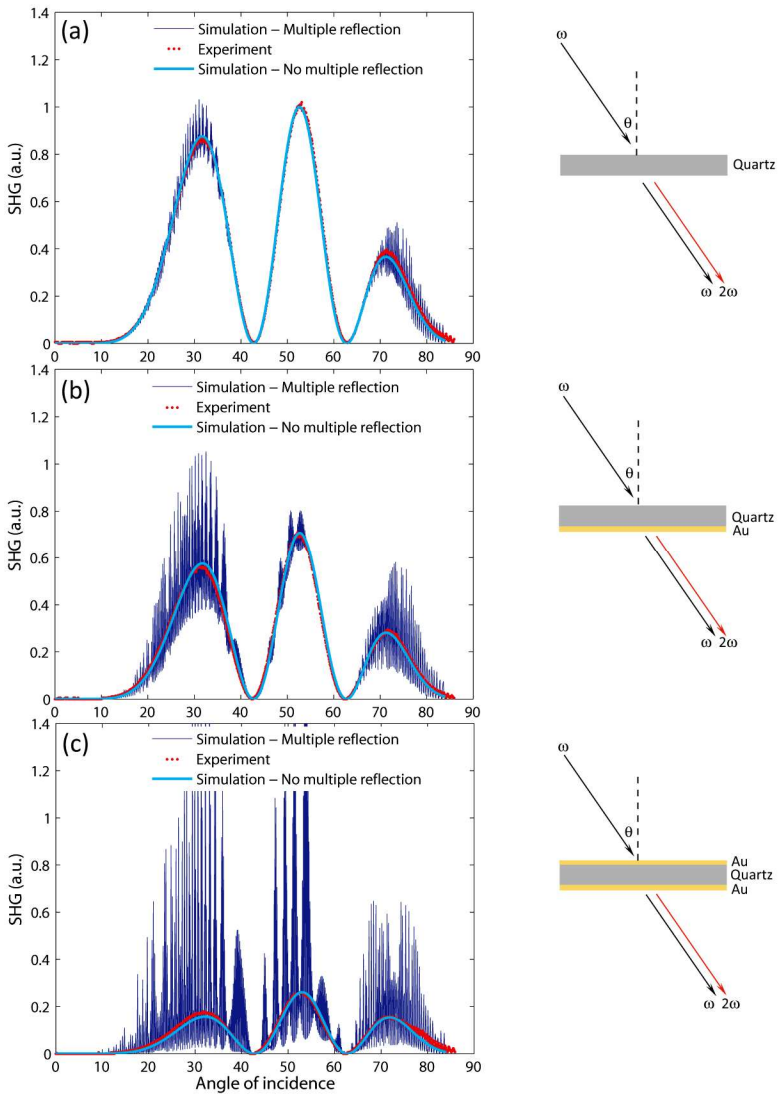

Fig. 2. Second harmonic intensities of X-cut quartz at varying angles of incidence in three cases (Rotation is about the *z* axis): (a) Quartz only, (b) Quartz/Au, and (c) Au/Quartz/Au. Experimental results (red dots) are plotted with two different simulated Maker fringe patterns (blue: multiple reflections, cyan: no multiple reflections).

gold layer. We note that the experimental Maker fringes showed a good agreement with simulations taking into account multilayer structures as shown in Figs. 2(b) and (c). Experimental curves in Figs. 2(b) and (c) show large difference in both SHG magnitude and fringe shape with that in Fig. 1(a) where no additional gold layers are present. This indicates that it is important to include multilayer structures in analysis. The same simulation result as the cyan curve in Fig. 1(a) is obtained from the HH method that is based on three layer structure. The SH multiple reflections included in the HH method also cannot contribute to the SHG because the beam size is small compared with the quartz thickness and multiply reflected SH beams cannot interfere with each other. Note that the experimental data deviate slightly from the theoretical estimation at large angles because, for a thick sample, the laser beam translates on the back surface during rotation and this introduces sensitivity to both surface and thickness variations.

#157751 - $15.00 USD Received 7 Nov 2011; revised 9 Dec 2011; accepted 12 Dec 2011; published 19 Dec 2011

A nonlinear polymer thin film was fabricated by doping 30 wt.% of AJL49, provided by the University of Washington, with an amorphous polycarbonate (APC) host. The nonlinear polymer solution was spin-coated on a 180 nm thick indium tin oxide (ITO)/glass substrate manufactured by Delta Technologies (Product #: CB-40IN-0111), to give a 1.2 μm thick film. Then 100 nm thick gold was deposited on the film using a thermal evaporator. After contact poling at the glass transition temperature of 135 °C using a poling voltage of ~100 V/μm, the gold poling electrode was etched off using a gold etchant KI + I_2 + H_2O (4:1:40) for a transmission type Maker fringe experiment. The optical properties of ITO and the NLOP film were measured using a spectroscopic ellipsometer (VASE®, J. A. Woollam Co., Inc.) as shown in Figs. 3(a) and (b). Note that the large linear absorption of ITO in the infrared region can lead to considerable back reflections of fundamental waves.

Multiply reflected beams inside a few micron thick NLOP film interfere because of the larger ratio of beam size to NLO film thickness. Therefore, back reflections of both fundamental and SH waves should be included in the analysis when back reflections at the interface of NLOP/TCO/substrate are not negligible. As shown in Figs. 3(c) and (d), our derived formulas in Eqs. (4) and (6) (cyan curve) agree very well with experimental results (red circles) in both $p \rightarrow p$ and $s \rightarrow p$ cases. Noteworthy is that one can see a slight dip around 50° angle of incidence caused by back reflections in both the experimental and simulation data. However, this dip is not accounted for properly when back reflections of fundamental waves are ignored (green dash and black curve), which demonstrates that back reflections of fundamental waves should be taken into account in the analysis of SH transmission. In fact,

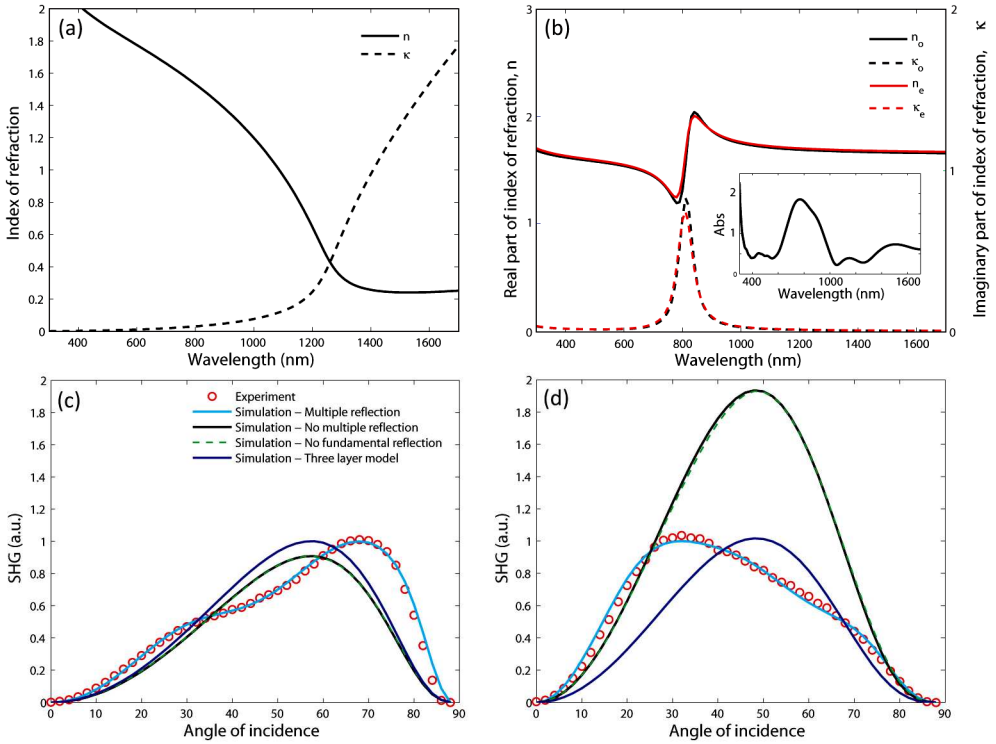

Fig. 3. (a) Complex index of refraction of ITO, (b) Complex anisotropic indices of refraction of NLOP measured using ellipsometer (inset figure: absorption profile of the multilayered sample by UV-VIS spectrophotometer), (c) $p \rightarrow p$ and (d) $s \rightarrow p$ Maker fringe profiles. Experimental results (red circles) were plotted with simulation results by various types of configurations. For line colors in (c) and (d), Cyan: multilayer structure with multiple reflections of both fundamental and SH. Black: multilayer structure without any multiple reflections. Green dash: multilayer structure with multiple reflections of SH only. Blue: three layer model (air/NLOP/substrate) without any multiple reflections.

#157751 - $15.00 USD Received 7 Nov 2011; revised 9 Dec 2011; accepted 12 Dec 2011; published 19 Dec 2011

the fundamental wave is more reflective than the SH at the ITO layer because of free carrier absorption of ITO in the infrared region as shown in Fig. 3(a). Depending on the thickness and optical properties of the NLOP film and the ITO layers, the shape and the dip position may change drastically. The linear absorption of the NLO film and the ITO is taken into account in the analysis based on the complex index of refraction in Figs. 3(a) and (b), but the nonparametric nonlinear absorption of the NLO film (imaginary part of *d*-tensor component) is ignored for this specific nonlinear polymer because it is expected to be small compared with the real part of the *d*-tensor component. The effect of a nonlinear absorption up to 20% of the real part of the *d*-tensor component in the analysis is negligible in the fitting results, whereas the linear absorption of ITO and NLO film does affect the fitting. We also see that the analysis by the three layer model (blue curves in Figs. 3(c) and (d)), ignoring back reflection terms, is not suitable for the analysis of Maker fringe data from the multilayered structures involving reflective layers. Therefore, inclusion of the back reflection of fundamental waves and multilayer structures in the analysis is crucial in order to reliably estimate SH *d*-tensor components for the poled polymer thin films.

For the AJL49 NLOP film, we measured a SH d_{33} of 360 ± 5 pm/V with the ratio of $d_{31}/d_{33} \cong 0.31$. Using the two-level model [24], the EO coefficient r_{33} is estimated to be 140 ± 30 pm/V and 100 ± 20 pm/V at 1300 nm and 1550 nm respectively, where the large error bound results from imprecise knowledge of local field effects. We were unable to directly measure EO coefficients of this sample, because the 1.2 μm thick film can support only one guided mode, which doesn't allow use of the Attenuated Total Reflection (ATR) method for an accurate characterization. Direct measurement of EO coefficients of a thicker AJL49/APC sample with the higher weight percentage of 45 wt.% and lower poling field of 70 V/μm gave an EO coefficient r_{33} of 110 pm/V and 80 pm/V at 1300 nm and 1550 nm, respectively, which are comparable to our estimation from the measured SH d_{33}.

4. Conclusions

We have presented new closed-form expressions for obtaining SH *d*-coefficients from Maker fringe SHG experiments on poled polymer thin films embedded in a multilayer structure with reflective layers, which can be dielectric or non-dielectric. The multilayer analysis including back reflections is necessary for second-order NLOP thin films prepared by electrode contact poling. We have shown that a TCO layer as a poling electrode has to be included in the analysis because it can enhance multiple reflections. We expect the proposed formulation to be useful to characterize Maker fringes of a multilayered poled polymer thin film or thick organic material [25] and to investigate the relation between SHG and EO properties on the same sample for contact poled films. Our formulations can also be applied to NLO crystals [26,27] by modifying, in a straightforward manner, the reflectance, transmittance, and effective *d* coefficients depending on the spatial symmetry and crystal cut.

Appendix A: Bound waves

We assume no pump depletion of the fundamental wave because, in the absence of phase matching, it is assumed to be negligible. From Maxwell's equations, the nonlinear wave equation in *cgs* unit convention is

$$\nabla\times\nabla\times\mathbf{E}_2-\left(2k_0\right)^2\begin{pmatrix} n_{2o}^2 & 0 & 0\\ 0 & n_{2o}^2 & 0\\ 0 & 0 & n_{2e}^2\end{pmatrix}\mathbf{E}_2=\left(2k_0\right)^2 4\pi\mathbf{P}^{NL}, \tag{A1}$$

where the nonlinear polarization is given by

$$\mathbf{P}^{NL}=\vec{\vec{\mathbf{d}}}:\mathbf{E}_1\mathbf{E}_1. \tag{A2}$$

Because the fundamental field $\mathbf{E}_1$ in Eq. (A2) contains both forward and backward electric fields resulting from multiple reflections, the SH field $\mathbf{E}_2$ inside the NLO film has three

#157751 - $15.00 USD Received 7 Nov 2011; revised 9 Dec 2011; accepted 12 Dec 2011; published 19 Dec 2011

particular solutions for the bound waves, $\mathbf{e}_b e^{2i\mathbf{k}_{1f}\cdot\mathbf{r}}$, $\mathbf{e}_b^r e^{2i\mathbf{k}_{1f}^r\cdot\mathbf{r}}$, and $\mathbf{e}_{mix} e^{i\left(\mathbf{k}_{1f}+\mathbf{k}_{1f}^r\right)\cdot\mathbf{r}}$ along with two homogeneous solutions $\hat{\mathbf{e}}_{2f} e^{i\mathbf{k}_{2f}\cdot\mathbf{r}}$ and $\hat{\mathbf{e}}_{2f}^r e^{i\mathbf{k}_{2f}^r\cdot\mathbf{r}}$ for the free waves. However, we neglect the last term $\mathbf{e}_{mix} e^{i\left(\mathbf{k}_{1f}+\mathbf{k}_{1f}^r\right)\cdot\mathbf{r}}$ because of the large phase mismatch. Two homogenous and two particular solutions are included in the field expressions in Eq. (2). Substituting $\mathbf{E}_2$ for the bound wave $\mathbf{e}_b$ or $\mathbf{e}_b^r$ and multiplying $\hat{\mathbf{e}}_{2f}$ or $\hat{\mathbf{e}}_{2f}^r$ in Eq. (A1) gives, after some algebraic manipulations (see Ref. [10]), the following relations:

$$n_{2f}(\theta_{2f})\cos\gamma_{2f} e_{bx} \pm \cos(\theta_{2f}-\gamma_{2f}) h_{by} = \frac{4\pi k_0 L}{\phi_1^{(\eta)} \mp \frac{1}{2}\phi_2^{(p)}} \begin{cases} \hat{\mathbf{e}}_{2f}\cdot\mathbf{P}^{NL} \\ \hat{\mathbf{e}}_{2f}^r\cdot\mathbf{P}^{NL} \end{cases} \tag{A3}$$

and

$$n_{2f}(\theta_{2f})\cos\gamma_{2f} e_{bx}^r \pm \cos(\theta_{2f}-\gamma_{2f}) h_{by}^r = \frac{4\pi k_0 L}{-\phi_1^{(\eta)} \mp \frac{1}{2}\phi_2^{(p)}} \begin{cases} \hat{\mathbf{e}}_{2f}\cdot\mathbf{P}^{NLr} \\ \hat{\mathbf{e}}_{2f}^r\cdot\mathbf{P}^{NLr} \end{cases}, \tag{A4}$$

where e_{bx} and h_{by} are x- and y-components of the forward bound electric and magnetic field, respectively, and the superscript r denotes the reflected bound field. The phase terms are $\phi_1^{(p)} = k_0 n_{1f}(\theta_{1f})\cos\left(\theta_{1f}\right)L$, $\phi_1^{(s)} = k_0 n_{1o}\cos\left(\theta_{1f}^{(s)}\right)L$, and $\phi_2^{(p)} = 2k_0 n_{2f}(\theta_{2f})\cos\left(\theta_{2f}\right)L$. The inner products of the unit vector nonlinear polarization in the right hand side of Eqs. (A3) and (A4) are given as

$$\begin{aligned}
\hat{\mathbf{e}}_{2f}\cdot\mathbf{P}^{NL} &= E_1^2 \hat{\mathbf{e}}_{2f}\cdot\vec{\mathbf{d}}:\hat{\mathbf{e}}_{1f}\hat{\mathbf{e}}_{1f} = -E_1^2 d_{eff}^{(p\to p)} \\
\hat{\mathbf{e}}_{2f}^r\cdot\mathbf{P}^{NL} &= E_1^2 \hat{\mathbf{e}}_{2f}^r\cdot\vec{\mathbf{d}}:\hat{\mathbf{e}}_{1f}\hat{\mathbf{e}}_{1f} = -E_1^2 d_{eff}^{r(p\to p)} \\
\hat{\mathbf{e}}_{2f}\cdot\mathbf{P}^{NLr} &= E_{1r}^2 \hat{\mathbf{e}}_{2f}\cdot\vec{\mathbf{d}}:\hat{\mathbf{e}}_{1f}^r\hat{\mathbf{e}}_{1f}^r = -E_{1r}^2 d_{eff}^{r(p\to p)} \\
\hat{\mathbf{e}}_{2f}^r\cdot\mathbf{P}^{NLr} &= E_{1r}^2 \hat{\mathbf{e}}_{2f}^r\cdot\vec{\mathbf{d}}:\hat{\mathbf{e}}_{1f}^r\hat{\mathbf{e}}_{1f}^r = -E_{1r}^2 d_{eff}^{(p\to p)},
\end{aligned} \tag{A5}$$

where the effective SH d-coefficients for forward and backward waves are

$$\begin{aligned}
d_{eff}^{(p\to p)} &= 2d_{15}c_{2-\gamma}s_{1-\gamma}c_{1-\gamma} + s_{2-\gamma}\left(d_{31}c_{1-\gamma}^2 + d_{33}s_{1-\gamma}^2\right) \\
d_{eff}^{r(p\to p)} &= -2d_{15}c_{2-\gamma}s_{1-\gamma}c_{1-\gamma} + s_{2-\gamma}\left(d_{31}c_{1-\gamma}^2 + d_{33}s_{1-\gamma}^2\right)
\end{aligned} \tag{A6}$$

with

$$c_{i-\gamma} = \cos(\theta_{if}-\gamma_{if}),\ s_{i-\gamma} = \sin(\theta_{if}-\gamma_{if}). \tag{A7}$$

For the $s \to p$ case, we have

$$d_{eff}^{(s\to p)} = d_{31}s_{2-\gamma} = d_{eff}^{r(s\to p)}. \tag{A8}$$

Note that if Kleinman symmetry is not valid ($d_{31} \neq d_{15}$), then an additional input and output polarization scheme, *e.g.* $\alpha \to s$ (α-polarized fundamental input to s-polarized SH), should be considered in order to determine d_{15} separately. In this case, the fundamental electric field inside nonlinear medium can be expressed as

$$\mathbf{E}_{1f} = E_{1s}\hat{\mathbf{y}}e^{i\mathbf{k}_{1f}^{s}\cdot\mathbf{r}} + E_{1s}^r\hat{\mathbf{y}}e^{i\mathbf{k}_{1f}^{s,r}\cdot\mathbf{r}} + E_{1p}\hat{\mathbf{e}}_{1p}e^{i\mathbf{k}_{1f}^{p}\cdot\mathbf{r}} + E_{1p}^r\hat{\mathbf{e}}_{1p}^r e^{i\mathbf{k}_{1f}^{p,r}\cdot\mathbf{r}}. \tag{A9}$$

Then, we obtain

#157751 - $15.00 USD Received 7 Nov 2011; revised 9 Dec 2011; accepted 12 Dec 2011; published 19 Dec 2011

$$\hat{\mathbf{y}}\cdot\vec{\mathbf{d}}:\mathbf{E}_{1f}\mathbf{E}_{1f}$$
$$=-2d_{15}s_{1-\gamma}\left(E_{1s}E_{1p}e^{i\left(\mathbf{k}_{1f}^{s}+\mathbf{k}_{1f}^{p}\right)\cdot\mathbf{r}}+E_{1s}E_{1p}^{r}e^{i\left(\mathbf{k}_{1f}^{s}+\mathbf{k}_{1f}^{p,r}\right)\cdot\mathbf{r}}+E_{1s}^{r}E_{1p}e^{i\left(\mathbf{k}_{1f}^{s,r}+\mathbf{k}_{1f}^{p}\right)\cdot\mathbf{r}}+E_{1s}^{r}E_{1p}^{r}e^{i\left(\mathbf{k}_{1f}^{s,r}+\mathbf{k}_{1f}^{p,r}\right)\cdot\mathbf{r}}\right), \quad \text{(A10)}$$

where we ignore terms such as $e^{i\left(\mathbf{k}_{1f}^{s}+\mathbf{k}_{1f}^{p,r}\right)\cdot\mathbf{r}}$ and $e^{i\left(\mathbf{k}_{1f}^{s,r}+\mathbf{k}_{1f}^{p}\right)\cdot\mathbf{r}}$ because they don't contribute to SHG. The *s*-polarized SH transmission coefficient for α-polarized fundamental input is given in Appendix C.

Appendix B: Boundary conditions

As the number of layers becomes larger, the analysis becomes more complicated. A matrix method facilitates solving complicated boundary conditions [22]. We use the 2×2 matrix method to obtain the equations resulting from the boundary conditions and calculate the SH transmission and reflection coefficients. Continuity of tangential **E** and **H** components at each interface provides boundary conditions, which can be expressed in the matrix form

$$\begin{aligned}
&\text{I/II}: \quad e^{i\phi_{2aB}}\mathbb{D}_a\begin{pmatrix}0\\ r_{a\to S}^{(p\to p)}\end{pmatrix}=\mathbb{D}_B\mathbb{P}_B\begin{pmatrix}A\\ B\end{pmatrix},\\
&\text{II/III}: \quad \mathbb{D}_B\begin{pmatrix}A\\ B\end{pmatrix}=\mathbb{D}_f\begin{pmatrix}C\\ D\end{pmatrix}+\begin{pmatrix}e_{bx}\\ h_{by}\end{pmatrix}+\begin{pmatrix}e_{bx}^{r}\\ h_{by}^{r}\end{pmatrix},\\
&\text{III/IV}: \quad \mathbb{D}_f\mathbb{P}_2^{-1}\begin{pmatrix}C\\ D\end{pmatrix}+e^{2i\phi_1}\begin{pmatrix}e_{bx}\\ h_{by}\end{pmatrix}+e^{-2i\phi_1}\begin{pmatrix}e_{bx}^{r}\\ h_{by}^{r}\end{pmatrix}=\mathbb{D}_T\mathbb{P}_{2TL}^{-1}\begin{pmatrix}E\\ F\end{pmatrix},\\
&\text{IV/V}: \quad \mathbb{D}_T\mathbb{P}_T^{-1}\mathbb{P}_{2TL}^{-1}\begin{pmatrix}E\\ F\end{pmatrix}=e^{i(\phi_{2SL}+\phi_{2ST})}\mathbb{D}_S\begin{pmatrix}t_{a\to S}^{(p\to p)}\\ 0\end{pmatrix},
\end{aligned} \quad \text{(B1)}$$

where the phase terms are $\phi_{2aB}=2k_0n_{2a}c_{2a}d_B$, $\phi_{2SL}=2k_0n_{2S}c_{2S}L$, and $\phi_{2ST}=2k_0n_{2S}c_{2S}d_T$. The dynamic and propagation matrices $\mathbb{D}$ and $\mathbb{P}$ are given as

$$\begin{aligned}
&\mathbb{D}_l=\begin{pmatrix}\cos(\theta_{2l}) & -\cos(\theta_{2l})\\ n_{2l} & n_{2l}\end{pmatrix},\ \mathbb{D}_f=\begin{pmatrix}\cos(\theta_{2f}-\gamma_{2f}) & -\cos(\theta_{2f}-\gamma_{2f})\\ n_2\cos(\gamma_2) & n_2\cos(\gamma_2)\end{pmatrix},\\
&\mathbb{P}_m=\begin{pmatrix}e^{-i\phi_{2m}} & 0\\ 0 & e^{i\phi_{2m}}\end{pmatrix},\ \mathbb{P}_f=\begin{pmatrix}e^{-i\phi_{2f}} & 0\\ 0 & e^{i\phi_{2f}}\end{pmatrix},\text{and }\mathbb{P}_{2TL}=\begin{pmatrix}e^{-i\phi_{2TL}} & 0\\ 0 & e^{i\phi_{2TL}}\end{pmatrix},
\end{aligned} \quad \text{(B2)}$$

where $l=a,B,T,S$ and $m=B,T$. The walk-off angle should be applied to the dynamic matrix when the layer is anisotropic as included in the matrix $\mathbb{D}_f$ for the nonlinear film. The phase terms are $\phi_{2m}=2k_0n_{2m}c_{2m}d_m$ ($m=B,T$) and $\phi_{2TL}=2k_0n_{2T}c_{2T}L$. From Eq. (B1), we can construct a matrix equation

$$\begin{aligned}
e^{i(\phi_{2SL}+\phi_{2ST})}\mathbb{D}_{a\to S}\begin{pmatrix}t_{a\to S}^{(p\to p)}\\ 0\end{pmatrix}&=e^{i\phi_{2aB}}\begin{pmatrix}0\\ r_{a\to S}^{(p\to p)}\end{pmatrix}-\frac{1}{2n_{2f}c_{\gamma_2}c_{2-\gamma}}\mathbb{D}_{aBf}\\
&\times\left\{\begin{pmatrix}1-e^{i(2\phi_1^{(p)}-\phi_2^{(p)})} & 0\\ 0 & 1-e^{i(2\phi_1^{(p)}+\phi_2^{(p)})}\end{pmatrix}\begin{pmatrix}n_{2f}c_{\gamma_2}e_{bx}+c_{2-\gamma}h_{by}\\ -n_{2f}c_{\gamma_2}e_{bx}+c_{2-\gamma}h_{by}\end{pmatrix}\right.\\
&\left.+\begin{pmatrix}1-e^{-i(2\phi_1^{(p)}+\phi_2^{(p)})} & 0\\ 0 & 1-e^{-i(2\phi_1^{(p)}-\phi_2^{(p)})}\end{pmatrix}\begin{pmatrix}n_{2f}c_{\gamma_2}e_{bx}^{r}+c_{2-\gamma}h_{by}^{r}\\ -n_{2f}c_{\gamma_2}e_{bx}^{r}+c_{2-\gamma}h_{by}^{r}\end{pmatrix}\right\},
\end{aligned} \quad \text{(B3)}$$

where $c_{\gamma_2}=\cos\gamma_{2f}$. The dynamic matrix for the multilayered stack is given as

#157751 - $15.00 USD Received 7 Nov 2011; revised 9 Dec 2011; accepted 12 Dec 2011; published 19 Dec 2011

$$\mathbb{D}_{aBf}=\frac{1}{t_{aBf}^{(2p)}}\begin{pmatrix}1 & -r_{fBa}^{(2p)}\\ r_{aBf}^{(2p)} & t_{aBf}^{(2p)}t_{fBa}^{(2p)}-r_{aBf}^{(2p)}r_{fBa}^{(2p)}\end{pmatrix},\ \mathbb{D}_{a\to S}=\frac{1}{t_{a\to S}^{(2p)}}\begin{pmatrix}1 & -r_{S\to a}^{(2p)}\\ r_{a\to S}^{(2p)} & t_{a\to S}^{(2p)}t_{S\to a}^{(2p)}-r_{a\to S}^{(2p)}r_{S\to a}^{(2p)}\end{pmatrix}. \quad \text{(B4)}$$

Assuming that the incident light is a plane wave, iteration of the Airy formula [21,22] gives the reflection and the transmission coefficients in the multilayered structure. The resulting expressions for reflection and transmission coefficient have the form

$$r_{a\to S}^{(i\eta)}=\frac{r_{aB}^{(i\eta)}+r_{B\to S}^{(i\eta)}e^{2i\beta_B^{(i\eta)}d_B}}{1+r_{aB}^{(i\eta)}r_{B\to S}^{(i\eta)}e^{2i\beta_B^{(i\eta)}d_B}}\Leftarrow r_{B\to S}^{(i\eta)}=\frac{r_{Bf}^{(i\eta)}+r_{fTS}^{(i\eta)}e^{2i\beta_f^{(i\eta)}L}}{1+r_{Bf}^{(i\eta)}r_{fTS}^{(i\eta)}e^{2i\beta_f^{(i\eta)}L}}\Leftarrow r_{iTS}^{(i\eta)}=\frac{r_{fT}^{(i\eta)}+r_{TS}^{(i\eta)}e^{2i\beta_T^{(i\eta)}d_T}}{1+r_{fT}^{(i\eta)}r_{TS}^{(i\eta)}e^{2i\beta_T^{(i\eta)}d_T}} \quad \text{(B5)}$$

and

$$t_{a\to S}^{(i\eta)}=\frac{t_{aB}^{(i\eta)}t_{B\to S}^{(i\eta)}e^{i\beta_B^{(i\eta)}d_B}}{1+r_{aB}^{(i\eta)}r_{B\to S}^{(i\eta)}e^{2i\beta_B^{(i\eta)}d_B}}\Leftarrow t_{B\to S}^{(i\eta)}=\frac{t_{Bf}^{(i\eta)}t_{fTS}^{(i\eta)}e^{i\beta_f^{(i\eta)}L}}{1+r_{Bf}^{(i\eta)}r_{fTS}^{(i\eta)}e^{2i\beta_f^{(i\eta)}L}}\Leftarrow t_{iTS}^{(i\eta)}=\frac{t_{fT}^{(i\eta)}t_{TS}^{(i\eta)}e^{i\beta_T^{(i\eta)}d_T}}{1+r_{fT}^{(i\eta)}r_{TS}^{(i\eta)}e^{2i\beta_T^{(i\eta)}d_T}}, \quad \text{(B6)}$$

where the *s*- and *p*- propagation constants are given by $\beta_l^{(is)}=i\cdot k_o n_s\cos(\theta_s)$ and $\beta_l^{(ip)}=i\cdot k_o n_p(\theta_p)\cos(\theta_p)$ and these can be applied at each layer with appropriate anisotropic indices and internal angles. n_p is given in Eq. (3), $n_s=n_o$, and θ_s and θ_p are the complex propagation angles inside the medium. The corresponding reflection and transmission coefficients from layer *j* to *k* are given by

$$r_{jk}^{(is)}=\frac{Z_k^{(is)}-Z_j^{(is)}}{Z_k^{(is)}+Z_j^{(is)}},\ r_{jk}^{(ip)}=\frac{Z_j^{(ip)}-Z_k^{(ip)}}{Z_j^{(ip)}+Z_k^{(ip)}},\ t_{jk}^{(i\eta)}=\frac{2Z_j^{(i\eta)}}{Z_j^{(i\eta)}+Z_k^{(i\eta)}}\frac{n_j(\theta_j)\cos\gamma_{ij}}{n_k(\theta_k)\cos\gamma_{ik}}\ , \quad \text{(B7)}$$

with the *s*- and *p*- wave impedances of each anisotropic and/or absorbing layer given by [28]

$$Z^{(is)}=\frac{1}{\sqrt{n_{io}^2-\sin^2\theta}},\ Z^{(ip)}=\frac{1}{n_{io}}\sqrt{1-\left(\frac{\sin\theta}{n_{ie}}\right)^2}, \quad \text{(B8)}$$

where θ is the external angle of incidence from air, and i = 1 or 2 represents fundamental and SH wavelengths, respectively. These can be applied to other layers with corresponding refractive indices and angle of incidence from air.

Appendix C: *α*-polarized fundamental to *s*-polarized SHG

We assume the input fundamental wave is polarized at an angle α (*e.g.* 0° and 90° mean *s*- and *p*-polarizations, respectively). Similar to the $p\to p$ calculations in Appendix B, we can solve boundary conditions such that E_y and H_x are continuous at each interface and obtain the *s*-polarized SH transmission coefficient in the form

$$t_{a\to S}^{(\alpha\to s)}=-e^{-2ik_0n_{2S}c_{2S}(L+d_T+l_{AD})}\frac{1}{2n_{2o}c_{2f}}\frac{t_{a\to S}^{(2s)}}{t_{a\to f}^{(2s)}}$$
$$\times\left[\begin{array}{l}\left(1-e^{i(\phi_1^{(s)}+\phi_1^{(p)}-\phi_2^{(s)})}\right)\left(n_{2o}c_{2f}e_{by}-h_{bx}\right)-r_{f\to a}^{(2s)}\left(1-e^{i(\phi_1^{(s)}+\phi_1^{(p)}+\phi_2^{(s)})}\right)\left(n_{2o}c_{2f}e_{by}+h_{bx}\right)\\ +\left(1-e^{-i(\phi_1^{(s)}+\phi_1^{(p)}+\phi_2^{(s)})}\right)\left(n_{2o}c_{2f}e_{by}^r-h_{bx}^r\right)-r_{f\to a}^{(2s)}\left(1-e^{-i(\phi_1^{(s)}+\phi_1^{(p)}-\phi_2^{(s)})}\right)\left(n_{2o}c_{2f}e_{by}^r+h_{bx}^r\right)\end{array}\right], \quad \text{(C1)}$$

where $c_{2f}=\cos\theta_{2f}^{(s)}$ and $\theta_{2f}^{(s)}$ is the refractive angle of *s*-polarized light inside the film. Substituting $\mathbf{E}_2$ for the bound wave $\mathbf{e}_{by}e^{i\left(\mathbf{k}_{1f}^s+\mathbf{k}_{1f}^p\right)\cdot\mathbf{r}}$ or $\mathbf{e}_{by}^r e^{i\left(\mathbf{k}_{1f}^{s,r}+\mathbf{k}_{1f}^{p,r}\right)\cdot\mathbf{r}}$ and taking the dot product with $\hat{\mathbf{e}}_{2f}^{s}=\hat{\mathbf{e}}_{2f}^{s,r}=\hat{\mathbf{y}}$ in Eq. (A1) gives

#157751 - $15.00 USD Received 7 Nov 2011; revised 9 Dec 2011; accepted 12 Dec 2011; published 19 Dec 2011

$$n_{2o}c_{2f}e_{by} \pm h_{bx} = \mp \frac{8\pi k_0 L}{\phi_1^{(s)} + \phi_1^{(p)} \pm \phi_2^{(s)}} \hat{\mathbf{y}} \cdot \mathbf{P}^{NL}, \tag{C2}$$

and

$$n_{2o}c_{2f}e_{by}^{r} \pm h_{bx}^{r} = \pm \frac{8\pi k_0 L}{\phi_1^{(s)} + \phi_1^{(p)} \mp \phi_2^{(s)}} \hat{\mathbf{y}} \cdot \mathbf{P}^{NLr}, \tag{C3}$$

where

$$\hat{\mathbf{y}} \cdot \mathbf{P}^{NL} = -2E_{1s}E_{1p}d_{15}s_{1-\gamma}, \quad \hat{\mathbf{y}} \cdot \mathbf{P}^{NLr} = -2E_{1s}^{r}E_{1p}^{r}d_{15}s_{1-\gamma}. \tag{C4}$$

The fundamental s and p electric fields, $E_{1\eta}$ and $E_{1\eta}^{r}$, inside the nonlinear medium can be calculated from the input fundamental wave and Airy's formula. Assuming the α-polarized input fundamental wave is $\mathbf{E}_{1a} = E_{1a}\left(\hat{\mathbf{y}}\cos\alpha + \hat{\mathbf{e}}_{1a}\sin\alpha\right)$, the electric fields for forward and backward fundamental waves inside the NLO film can be expressed as

$$\begin{aligned}
\mathbf{E}_{1f} &= E_{1a}\left(\hat{\mathbf{y}}\cos\alpha\frac{t_{a\to S}^{(1s)}}{t_{f\to S}^{(1s)}}e^{-i\phi_1^{(s)}} + \hat{\mathbf{e}}_{1f}\sin\alpha\frac{t_{a\to S}^{(1p)}}{t_{f\to S}^{(1p)}}e^{-i\phi_1^{(p)}}\right) = \hat{\mathbf{y}}E_{1s} + \hat{\mathbf{e}}_{1f}E_{1p} \\
\mathbf{E}_{1f}^{r} &= E_{1a}\left(\hat{\mathbf{y}}\cos\alpha\frac{t_{a\to S}^{(1s)}}{t_{f\to S}^{(1s)}}r_{fTS}^{(1s)}e^{i\phi_1^{(s)}} + \hat{\mathbf{e}}_{1f}^{r}\sin\alpha\frac{t_{a\to S}^{(1p)}}{t_{f\to S}^{(1p)}}r_{fTS}^{(1p)}e^{i\phi_1^{(p)}}\right) = \hat{\mathbf{y}}E_{1s}^{r} + \hat{\mathbf{e}}_{1f}^{r}E_{1p}^{r}.
\end{aligned} \tag{C5}$$

Substitution into Eq. (C4) gives

$$\begin{aligned}
\hat{\mathbf{y}} \cdot \mathbf{P}^{NL} &= -\left(E_{1a}\right)^2 \sin\left(2\alpha\right)\frac{t_{a\to S}^{(1s)}}{t_{f\to S}^{(1s)}}\frac{t_{a\to S}^{(1p)}}{t_{f\to S}^{(1p)}}e^{-i\phi_1^{(s)}}e^{-i\phi_1^{(p)}}d_{15}s_{1-\gamma} \\
\hat{\mathbf{y}} \cdot \mathbf{P}^{NLr} &= -\left(E_{1a}\right)^2 \sin\left(2\alpha\right)\frac{t_{a\to S}^{(1s)}}{t_{f\to S}^{(1s)}}\frac{t_{a\to S}^{(1p)}}{t_{f\to S}^{(1p)}}r_{f\to S}^{(1s)}r_{f\to S}^{(1p)}e^{i\phi_1^{(s)}}e^{i\phi_1^{(p)}}d_{15}s_{1-\gamma}.
\end{aligned} \tag{C6}$$

From Eqs. (C2)-(C6), we thus obtain the s-polarized SH transmission coefficient in a similar form to Eq. (7):

$$\begin{aligned}
t_{a\to S}^{(\alpha\to s)} = -e^{-2ik_0 n_{2S}c_{2S}\left(L+d_T+l_{AD}\right)}\frac{4\pi i k_0 L}{n_{2o}c_{2f}}\left[\frac{t_{a\to S}^{(1s)}}{t_{f\to S}^{(1s)}}\frac{t_{a\to S}^{(1p)}}{t_{f\to S}^{(1p)}}E_{1a}^2\right]\frac{t_{a\to S}^{(2s)}}{t_{a\to f}^{(2s)}}\sin\left(2\alpha\right) \\
\times d_{15}s_{1-\gamma}\left\{\begin{aligned}&\left[e^{-i\Phi^{(\alpha\to s)}} + r_{f\to a}^{(2s)}\left(r_{f\to S}^{(1s)}r_{f\to S}^{(1p)}\right)e^{i\Phi^{(\alpha\to s)}}\right]\sin c\left(\Psi^{(\alpha\to s)}\right) \\ &+\left[e^{i\Psi^{(\alpha\to s)}}\left(r_{f\to S}^{(1s)}r_{f\to S}^{(1p)}\right) + r_{f\to a}^{(2s)}e^{-i\Psi^{(\alpha\to s)}}\right]\sin c\left(\Phi^{(\alpha\to s)}\right)\end{aligned}\right\},
\end{aligned} \tag{C7}$$

where $\Psi^{(\alpha\to s)}$ and $\Phi^{(\alpha\to s)}$ are defined as

$$\Psi^{(\alpha\to s)} = \frac{\phi_1^{(s)} + \phi_1^{(p)} - \phi_2^{(s)}}{2}, \quad \Phi^{(\alpha\to s)} = \frac{\phi_1^{(s)} + \phi_1^{(p)} + \phi_2^{(s)}}{2}. \tag{C8}$$

For the cases that α = 0° ($s\to s$) and α = 90° ($p\to s$) for the input polarization, Eq. (C7) gives the well-known result of zero SH intensity because of the sin(2α) term in Eq. (C7).

Acknowledgments

We would like to thank Professor Alex K.-Y. Jen and Dr. Jingdong Luo at the University of Washington for providing the nonlinear polymers.

#157751 - $15.00 USD Received 7 Nov 2011; revised 9 Dec 2011; accepted 12 Dec 2011; published 19 Dec 2011